Swiss J Geosci (2014) 107:293–307
DOI 10.1007/s00015-014-0169-5

Timing of retreat of the Reuss Glacier (Switzerland) at the end of the Last Glacial Maximum

Regina Reber · Naki Akçar · Susan Ivy-Ochs · Dmitry Tikhomirov · Reto Burkhalter · Conradin Zahno · Aron Lüthold · Peter W. Kubik · Christof Vockenhuber · Christian Schlüchter

Received: 21 November 2013 / Accepted: 17 September 2014 / Published online: 5 November 2014

Abstract We used cosmogenic ^{10}Be and ^{36}Cl to establish the timing of the onset of deglaciation after the Last Glacial Maximum of the Reuss Glacier, one of the piedmont lobes of the Alpine ice cap that reached the northern Alpine foreland in Switzerland. In this study, we sampled erratic boulders both at the frontal position in the foreland (Lenzburg and Wohlen, canton Aargau) and at the lateral Alpine border position (Seeboden moraine, Rigi, canton Schwyz). The minimum age for the beginning of retreat is 22.2 ± 1.0 ka at the frontal (terminal) position and 20.4 ± 1.0 ka at the lateral position. These ages are directly comparable with exposure ages from the other piedmont lobes in the northern Alpine foreland. Our data from the mountain called Rigi, do not support the hypothesis that boulders located external to the Seeboden moraine were deposited prior to the last glacial cycle. We present a first exposure age from an erratic boulder in a retreat position in the Alpine foreland. The Reuss Glacier was approximately 12 km behind the maximal extent no later than at 18.6 ± 0.9 ka.

Keywords Pleistocene · Northern Alpine foreland · Deglaciation · Erratic boulders · Surface exposure dating (^{10}Be, ^{36}Cl)

Electronic supplementary material The online version of this article (doi:10.1007/s00015-014-0169-5) contains supplementary material, which is available to authorized users.

R. Reber (✉) · N. Akçar · D. Tikhomirov · C. Schlüchter
Institute of Geological Sciences, University of Bern, Baltzerstrasse 1+3, 3012 Bern, Switzerland
e-mail: rreber@geo.unibe.ch

S. Ivy-Ochs · P. W. Kubik · C. Vockenhuber
Laboratory of Ion Beam Physics (LIP), ETH Zurich, 8093 Zurich, Switzerland

R. Burkhalter
Landesgeologie, Bundesamt für Landestopografie swisstopo, 3084 Wabern, Switzerland

C. Zahno
Sunnebergliweg 6, 6403 Küssnacht, Switzerland

A. Lüthold
CSD Ingenieure AG, Postfach, 6460 Altdorf, Switzerland

1 Introduction

The Last Glacial Maximum (LGM) describes the peak of the last glacial period between 26.5 ka and 19–20 ka (Clark et al. 2009), when ice sheets and glaciers reached their maximum extent for the last time. Global expansion of ice started between 33.0 and 26.5 ka (Clark et al. 2009). This evolution is archived both in marine and terrestrial sediments and culminated in the LGM (Starnberger et al. 2011 and references therein), which is time-correlated with the last sea-level minimum (Lambeck and Chappell 2001; Clark et al. 2009). Mix et al. (2001) placed the timing of this global signal at 21.0 ± 2.0 ka, based on the existing knowledge, whereas Shakun and Carlson (2010) give an age of 22.1 ± 4.3 ka for the LGM in the northern hemisphere.

The extent of LGM ice in the Alps and on the northern Alpine foreland is reconstructed based on mapping and detailed study of both morphological and sedimentological evidence such as glaciofluvial sediments, moraines and erratic boulders (Penck and Brückner 1901/1909; Beck 1933; Jäckli 1970; Schlüchter 2004; Bini et al. 2009). The petrographic composition of the sediments is used to fingerprint the different accumulation areas of the piedmont glaciers (e.g. Heim 1919; Hantke 1983; Graf 2009).

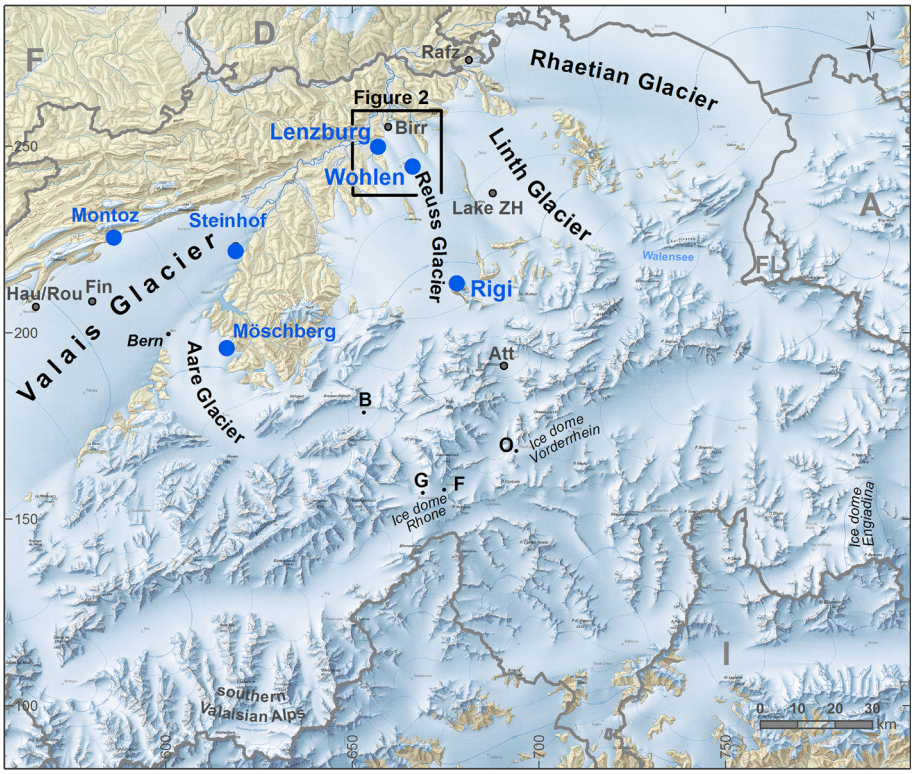

Fig. 1 Alpine ice extent at the Last Glacial Maximum (LGM) with major ice domes and piedmont glacier lobes (Bini et al. 2009) © Federal Office of Topography, swisstopo, CH-3084 Wabern. Ice transfluences are B: Brünigpass, F: Furkapass, G: Grimselpass and O: Oberalppass. Sample sites referred to in the text: Möschberg, Montoz, Steinhof. Sample sites (with boulder samples) of this study: Rigi (Rigi-1 to -9), Lenzburg (Reuss-21 and -22) and Wohlen (Reuss-20). Locations mentioned in the text: *Birr* Birrfeld; *Fin* Finsterhennen; *Rafz* Rafzerfeld; *Lake ZH* (*Zürich*) *and Hau/Rou* Hauterive/Rouges-Terres. *F* France, *D* Germany, *A* Austria; *FL* Liechtenstein, *I* Italy

Trimlines are also mapped to determine the LGM ice extent in the high Alpine valleys (Florineth and Schlüchter 1998; Kelly et al. 2004; Hippe et al. 2014). This mapping shows that the Alpine ice cap consisted of ice domes interconnected by transection valley glaciers which fed huge foreland piedmont lobes (Jäckli 1962; Bini et al. 2009).

The lobes in the Swiss sector of the northern Alpine foreland are from west to east: (1) the Valais Glacier (formerly known as the Rhône Glacier); (2) the Aare Glacier; (3) the Reuss Glacier; (4) the Linth Glacier and (5) the Rhaetian Glacier (formerly known as the Rhine Glacier; Bini et al. 2009). The Valais and the Rhaetian Glaciers were the two dominant piedmont lobes in the northern Alpine foreland, which were directly fed by outflow from the dome areas (Schlüchter 2004). The Reuss Glacier was situated between the Valais lobe and the Linth Glacier. The accumulation area of the Valais Glacier was the glacier plateau of the central Alps (Kelly et al. 2004), the ice dome Rhone and the high-altitude catchment areas of the southern Valaisian Alps (Bini et al. 2009; Fig. 1). The main sources for the Rhaetian Glacier were the ice domes Engiadina in the southeast of Switzerland and the ice dome Vorderrhein (Bini et al. 2009; Fig. 1). The Aare Glacier was fed by the catchment of the upper Aare valley but also from the ice dome Rhone by a transfluence to the north, across Grimselpass (G in Fig. 1). The Aare Glacier joined the Valais Glacier at the maximum extent near Bern (Baltzer 1896). The origin of the Reuss Glacier is the upper Reuss valley which received ice as well across Furkapass (F in Fig. 1) from the ice dome Rhone in the west and from a second branch across Oberalppass (O in Fig. 1) from the ice dome Vorderrhein in the east. Further downstream, ice from the Aare Glacier catchment contributed to the Reuss Glacier over Brünigpass (B in Fig. 1). The Linth Glacier was, in this period, rather a Linth-Rhine Glacier, because it was not only fed by the ice from the catchment of the Linth river, but also by a tributary branch of the Rhaetien Glacier that went through the Walensee trough (Bini et al. 2009).

The LGM in the central and the eastern Alps is dated between 30 and 18 ka, and thus occurred during MIS 2 (Keller and Krayss 2005b; Ivy-Ochs et al. 2008 and references therein). At that time, the margins of the piedmont glaciers fluctuated so that there may have been more than one advance to the furthest extent (van Husen 1997; Ellwanger et al. 1999; Keller and Krayss 2005a; Graf 2009). In the southern Alpine foreland, Monegato et al. (2007) identified two advances; the first between 26.5 and 23 cal ka BP and the second between 24 and 21 cal ka BP in the Tagliamento morainic amphitheater. Also Graf (2009) proposes a twofold LGM advance for the piedmont lobes in northern Switzerland based on lithostratigraphic evidence in the area of the Reuss Glacier. In the western part of the Reuss lobe, glaciofluvial deposits of the earlier

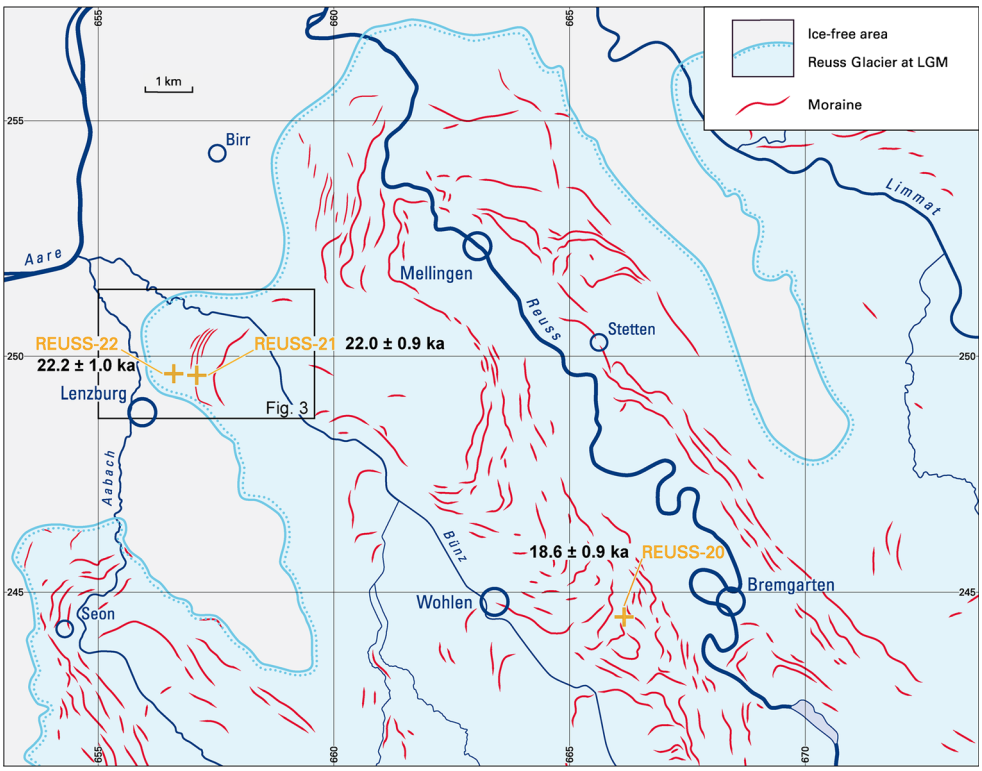

Fig. 2 Glacial morphological map of the frontal (terminal) part of the Reuss Glacier (LGM = Last Glacial Maximum). © Federal Office of Topography, swisstopo, CH-3084 Wabern. *Box* indicates the location of Fig. 3. Sample locations are *marked* with a *yellow cross* accompanied by the results of surface exposure dating. For location of the map area, see Fig. 1

Lindmühle advance (around 29 ka) locally lie beyond deposits of the younger Birmenstorf advance. Both reference localities, Lindmühle and Birmenstorf, are situated in the Birrfeld area (Birr in Fig. 1). These observations raise questions not only about the number of advances during the LGM but also on the synchrony of reconstructed maximum positions of the different oscillating piedmont lobes during this long cold period.

During the Birmenstorf advance the Reuss Glacier built up terminal moraines at its frontal position near Lenzburg at around 450 m a.s.l. (Graf 2009; Figs. 2, 3). Meanwhile, about 50 km upglacier from the terminus in Lenzburg, the same glacier deposited lateral moraines on the slopes of the mountain called Rigi at an elevation 500 m higher than the terminal moraines (e.g. Heim 1919; Hantke 2011; Figs. 1, 4). At the end of the LGM, retreat of the Reuss Glacier resulted in the construction of recessional moraines near Wohlen (canton Aargau) in frontal and at Rigi in lateral positions (Figs. 1, 2, 3, 4).

Here we address the questions of synchronity of LGM frontal and lateral positions, of differentiation of LGM and pre-LGM phenomena on the Rigi and of the potential use of polymict conglomerates for surface exposure dating. We collected samples from erratic boulders to answer these questions (1) on the terminal moraine near Lenzburg; (2) on the retreat stadial moraine near Wohlen; and (3) on lateral and recessional moraines on the Rigi. LGM and pre-LGM phenomena on the Rigi are complex and required sampling of boulders beyond the Seeboden moraine (Hantke 2006; Kopp 1953; Fig. 4).

2 Study sites and sample descriptions

2.1 Frontal (terminal) position at Lenzburg

The Lenzburg site is located in the Bünz valley (Fig. 2). The landscape here has been strongly modified by agricultural and building activities since Roman times (e.g. Krüger 2008). Relicts of glacial landforms, such as low-relief moraines, are primarily preserved in woodland that, most likely, has never been deforested. A high-resolution digital elevation model (DEM) shows faint glacigenic landforms to the north and just beyond the most distal moraine ridge that is easily visible in the field (red lines in Fig. 3). Therefore, DEM analysis allows reconstruction of an advanced LGM ice margin (blue line in Fig. 3) that is slightly farther out than that shown on the map from Bini et al. (2009). We interpret the terraces along the Bünz valley as being erosive forms in outwash deposits related to post-LGM recessional phases. Several generations of terraces along the Bünz are visible on the DEM.

There are only two granitic boulders of glacier origin at Lenzburg, most likely originating from the Aare massif. They have been selected for sampling because they are of granitic lithology and also large, rising more than 3 m

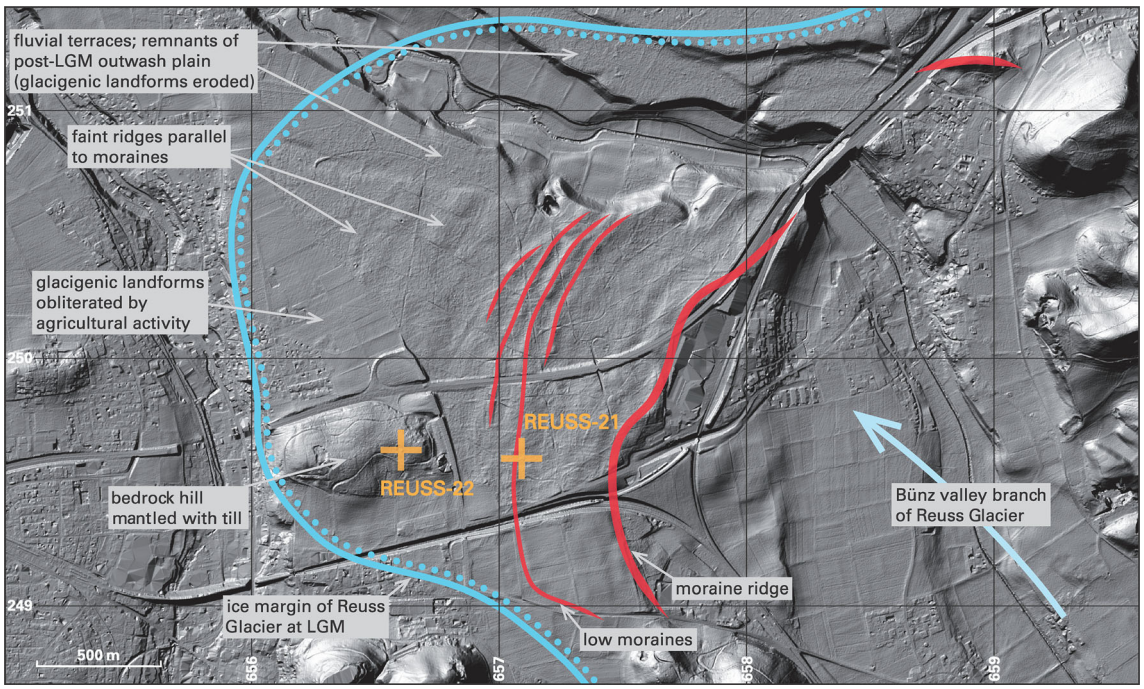

Fig. 3 The ice margin of the LGM Reuss Glacier (*blue*), with individual moraine ridges *marked* in *red*. Digital elevation model with 2 m resolution (DEM). © Federal Office of Topography, swisstopo, CH-3084 Wabern. For location of map area, see Fig. 2. *LGM* Last Glacial Maximum

above ground surface (Table 1; Fig. 5b, c). Field evidence shows boulder position stability since deposition (firm embedding). The local names for these solitary erratics are "Grosser Römerstein" (Reuss-21) and "Kleiner Römerstein" (Reuss-22; Jäckli 1966; Fig. 3). The position of the two boulders in this subdued glacial landscape is relevant to give a minimum age for the Birmenstorf advance sensu Graf (2009): Reuss-22 is situated on a till-mantled bedrock knoll, about 500 m inside the advanced LGM ice margin as reconstructed from the DEM, and Reuss-21 is on one of the moraines visible in the field (Fig. 3). Grosser Römerstein (Reuss-21; Fig. 5c) bears evidence of (Roman?) quarrying. However, the true sample location on the boulder top is considered to be undisturbed.

2.2 Lateral position on the Rigi

Rigi is a mountain located in the thrust belt of the Subalpine Molasse made of Late Paleogene proximal, alluvial fan conglomerates (Schlunegger et al. 1997 and references therein). The top of the mountain (1,798 m a.s.l.) is considered to have been a nunatak during the LGM (e.g. Heim 1919; Hantke 2006). The position of the Rigi with its exceptional lateral moraines is important for the reconstruction of the LGM outflow glaciers of the Alpine ice cap (Fig. 1).

Local morphology is likely evidence for glacier modification of parts of the mountain (Kopp 1953; Bini et al. 2009; Lüthold 2010; Fig. 4b) and small glaciers may have been present during the Last Glacial Maximum (e.g. Kopp 1953). Hantke (2006) draws the LGM ice margin at the Seeboden moraine (Fig. 4a) and as a consequence external glacial sediments would have to be deposited before the LGM (cf. Preusser et al. 2011). These external deposits contain erratic lithologies and therefore exclude local glacial transport only.

At the location Rigi, seven erratic boulders of various lithologies were sampled in the upper part of the slope (Figs. 4). Four of them are located on the Seeboden moraine (Rigi-2, -7, -8 and -9). Three boulders (Rigi-1, -5 and -6) were sampled externally to and topographically higher than the Seeboden moraine. These samples are from the morphologically complex slope externally of the Seeboden moraine (Figs. 4, 6, 7; Table 1). Sample Rigi-5 is from a limestone boulder (Early Cretaceous Schrattenkalk) and samples Rigi-6 to -9 are from polymict Molasse Nagelfluh (Hantke 2006). The petrographic composition of the conglomeratic boulders sampled is different from the directly underlying Molasse bedrock (Lüthold 2010). Samples Rigi-5 to -9 are collected and analysed to advance surface exposure dating methodology.

2.3 LGM recessional positions at Wohlen and at Rigi

Wohlen is located southeast of Lenzburg (Fig. 2). At this site, the moraines are attributed to a recessional complex of the Reuss Glacier (Stetten Stadial sensu Jäckli 1966). The

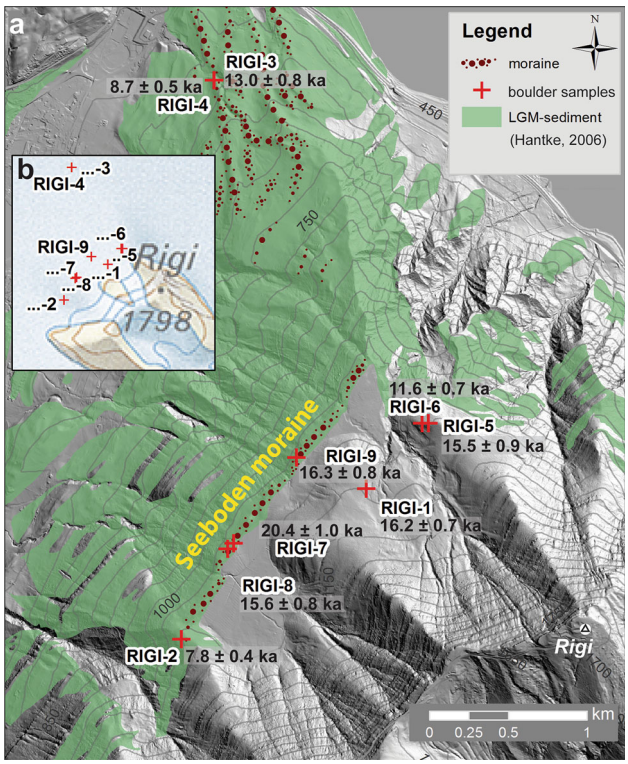

Fig. 4 **a** Glacial deposits on the northern slope of the Rigi (after Hantke 2006). Digital elevation model (DEM). © Federal Office of Topography, swisstopo, CH-3084 Wabern. Samples Rigi-7 to -9 are on the Seeboden moraine, Rigi-1, -5 and -6 are boulders above the Seeboden moraine, Rigi-3 and -4 are from boulders below the Seeboden moraine. **b** Crop of *LGM* Last Glacial Maximum map with extent of the Reuss Glacier (after Bini et al. 2009)

glacier terminus here was around 12 km short of the LGM ice margin (Fig. 2). Sample Reuss-20 is from a boulder on top of a recessional moraine, next to the "Erdmannlistein" (Fig. 5a; Heim 1919). The lithology is granitic, most likely originating from the Aare massif. The reason for sampling this boulder is to determine the timing of the first reorganisation of the Reuss Glacier during decay of the LGM ice.

Also on the Rigi the decaying Reuss Glacier produced recessional moraines at successively lower elevations at approximately 500 m below the Seeboden moraine (Hantke 2006; Lüthold 2010). The erratics Rigi-3 and -4 are situated on one of these moraines (Figs. 4, 6c; Table 1). They were collected for comparison with Reuss-20, both in post-LGM retreat positions.

3 Surface exposure dating

The synchrony of the oscillations of the several piedmont lobes can only be detected if terrestrial sediments related to glacier advances of the individual lobes are accurately dated (Ivy-Ochs and Kober 2008; Dunai 2010 and references therein). Surface exposure dating of an erratic boulder on a moraine, which marks the position of the former ice margin, yields the time of the boulder deposition or the beginning of moraine degradation and hence the specific advance (e.g. Porter and Swanson 2008). The advantage of surface exposure dating is the direct chronological positioning of a defined sedimentary fraction deposited directly by the glacier without any need for organic material. In most cases organic material is not available in sufficient quantities in glacigenic sediments; this natural deficit gives the cosmogenic nuclide dating an unmatched advantage.

The unstable cosmogenic isotopes ^{10}Be, ^{14}C, ^{26}Al, and ^{36}Cl, and stable cosmogenic isotopes ^{3}He and ^{21}Ne are produced in situ within the mineral lattices by interaction of a target atom with cosmic rays (Lal 1988). The exposure time of a rock surface can be calculated by determining the accumulated concentration of an isotope; assuming that the correct production rate and the amount of isotope inherited prior to exposure are known (e.g. Phillips et al. 1990).

Our samples were collected with hammer and chisel from large boulder tops following the strategies defined in Akçar et al. (2011). The samples were prepared at the Surface Exposure Laboratory of the University of Bern with nuclide specific procedures, and isotope concentrations were measured at the Laboratory of Ion Beam Physics at the Swiss Federal Institute of Technology (ETH) in Zurich, with accelerator mass spectrometry (AMS). Seven samples from granitic boulders were prepared for cosmogenic ^{10}Be and five samples (four conglomerates and one limestone) for cosmogenic ^{36}Cl.

3.1 Analysis of cosmogenic ^{10}Be

The target mineral for ^{10}Be ($t_{1/2} = 1.39 \pm 0.01$ Ma; Korschinek et al. 2010; Chmeleff et al. 2010) analysis is quartz. Cosmogenic ^{10}Be in quartz is produced through spallation reactions and muon capture on oxygen. For this reason, the first step is to extract and purify quartz out of the samples (Kohl and Nishiizumi 1992; Ivy-Ochs et al. 1996; Akçar 2006). Purified quartz from the seven samples was processed following the lab protocol in Akçar et al. (2012). Before dissolving the pure quartz sample with concentrated HF, it was spiked with 0.15–0.20 mg ^{9}Be. Be and Al were separated and purified via ion exchange columns. The samples were co-precipitated with iron, mixed with $AgNO_3$ solution and oxidized for AMS measurements (Akçar et al. 2012).

The weighted average ^{10}Be/^{9}Be full process blank ratio was $(2.90 \pm 0.33) \times 10^{-15}$. The contribution of the blank correction is less than 1.3 % for all samples. ^{10}Be exposure ages were calculated with the CRONUS-Earth online calculator of Balco et al. (2008; http://hess.ess.washington.

Table 1 Sample descriptions

Sample name	Lithology	Altitude (m)	Latitude, °N (DD.DD WGS84)	Longitude, °E (DD.DD WGS84)	Boulder height (cm)	Sample thickness (cm)	Thickness correction factor[a]	Shielding correction factor[b]
Reuss-20	Granitic	502	47.34763	8.31435	130	4	0.9676	1
Reuss-21	Granitic	446	47.39520	8.19465	450	5	0.9597	1
Reuss-22	Granitic	475	47.39550	8.18832	350 dh120	3	0.9756	1
Rigi-1	Granitic	1,099	47.06427	8.46774	70	5	0.9597	0.9874
Rigi-2	Granitic	1,064	47.05581	8.45214	145	3	0.9756	0.9839
Rigi-3	Granitic	535	47.08772	8.45548	150	4	0.9676	0.9990
Rigi-4	Granitic	536	47.08772	8.45548	200	5	0.9597	0.9990
Rigi-5	Limestone	1,100	47.06798	8.47299	60	4	0.9670	0.9941
Rigi-6	Conglomerate	1,095	47.06797	8.47248	160	4	0.9670	0.9913
Rigi-7	Conglomerate	1,030	47.06094	8.45611	320	4	0.9670	0.9924
Rigi-8	Conglomerate	1,030	47.06125	8.45661	120	4	0.9670	0.9924
Rigi-9	Conglomerate	1,035	47.06611	8.46196	370	2	0.9833	0.9953

dh difference of height from top of the boulder to nearest sediment cover

[a] Correction for sample thickness was done after Gosse and Phillips (2001), with mean attenuation length of 160 g cm^{-2} and rock density of 2.65 g cm^{-3}

[b] Calculated for topographic shielding and dip of the surface, after Dunne et al. (1999)

edu/math/ using wrapper script 2.2, main calculator 2.1, constants 2.2.1 and muons 1.1 with a user-supplied calibration data set for production rate calibration; Name: northeastern North America (NENA)—Developmental version. June 2009; Balco et al. (2009) as published by Balco in October 2013). Today, this is the best estimate for the northern hemisphere production rate (Fenton et al. 2011; Briner et al. 2012; Goehring et al. 2012; Young et al. 2013). Altitude/latitude scaling of the production rate was done according to the time dependent scheme (Lal 1991; Stone 2000) using a spallogenic SLHL (sea level—high latitude [>60°]) production rate of 3.88 ± 0.19 atoms g^{-1} SiO_2 a^{-1} (Balco et al. 2009). Rock density was taken as 2.65 g cm^{-3}. The shielding factors due to surrounding topography and thickness of the samples were calculated following Dunne et al. (1999b) using an exponential attenuation length of 160 g cm^{-2}. An erosion rate of 1.0 mm ka^{-1} was assumed (cf. André 2002), whereas the correction for vegetation and snow cover was excluded. The resulting data for the samples dated with ^{10}Be are given in Table 2.

3.2 Analysis of cosmogenic ^{36}Cl

The analysis of cosmogenic ^{36}Cl is given here in more detail than for ^{10}Be for the simple reason that the use for ^{36}Cl for conglomerates is at an experimental level. Major production channels of cosmogenic ^{36}Cl ($t_{1/2} = 301$ ka) for carbonates are fast neutron and muon spallation reactions on ^{40}Ca, capture of negative muons by ^{40}Ca and capture of thermal and epithermal neutrons by ^{35}Cl (Alfimov and Ivy-Ochs 2009 and references therein). Due to these multiple production channels in carbonates and additional channels in non-carbonate parts, ^{36}Cl sample preparation of a mixed conglomerate with carbonate and non-carbonate parts requires additional procedures in comparison to pure carbonate samples. Aliquots for elemental analysis were taken during ^{36}Cl sample preparation. Pure carbonate samples require only one solid aliquot that is taken after leaching of the sample. After the aliquot is taken, the carbonate sample is totally dissolved with nitric acid. As siliceous components in a conglomerate sample cannot be totally dissolved in nitric acid, two aliquots are needed to measure the elemental composition of the dissolved carbonate part of the conglomerate: a solid grain aliquot of the leached sample and a solid grain aliquot of the undissolved residue.

Among our samples, one was a pure carbonate and four were conglomerates with carbonate parts (Table 1). Major and trace elemental analysis for aliquots of these samples were done at SGS Mineral Services, Toronto, Canada (Online Resource 1). Before taking the first aliquots, all samples were crushed and sieved and only the fraction 0.250–0.400 mm was processed further using the sample preparation procedure described by Ivy-Ochs et al. (2004b). Samples were leached twice overnight in solution of 75 ml of HNO_3 (2M) in 500 ml ultrapure water (18.2 MΩ cm) and then rinsed ten times with ultrapure water to remove atmospheric ^{36}Cl. Each sample was spiked with about 2.5 mg of pure ^{35}Cl and then dissolved with

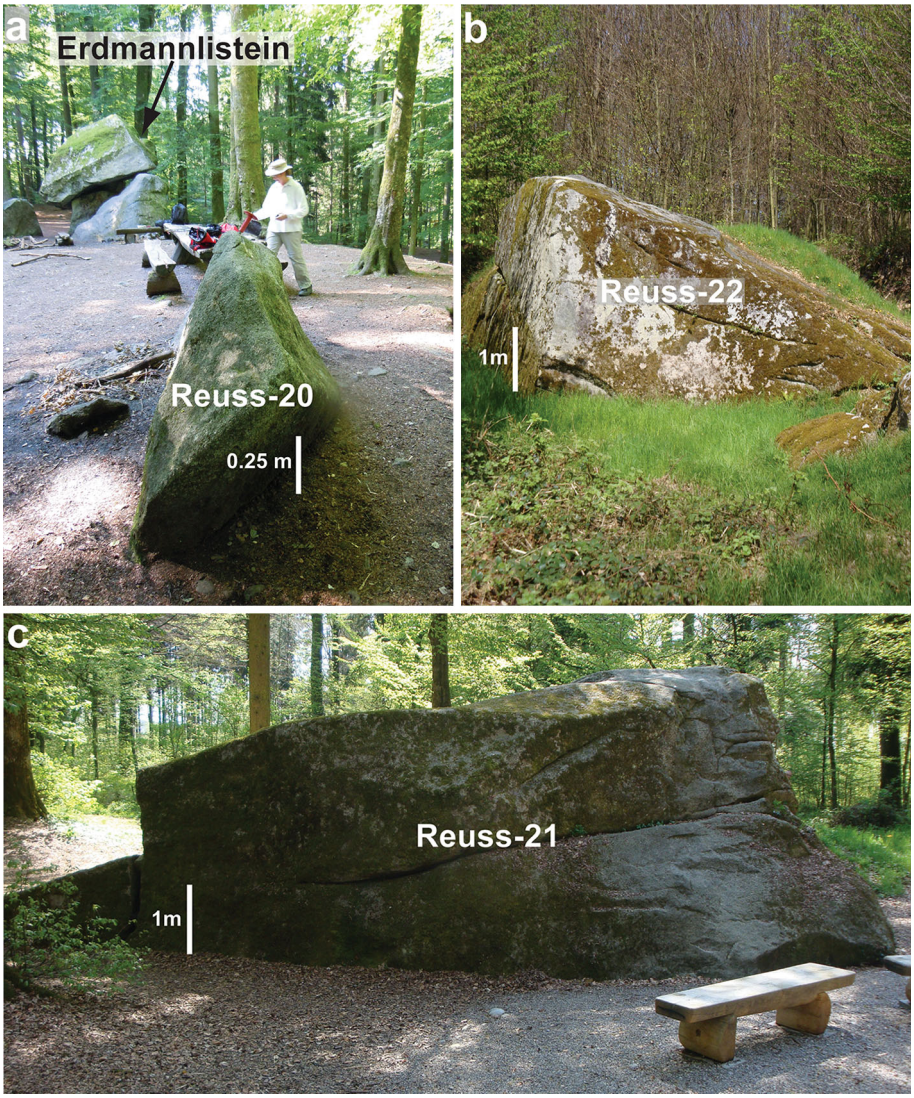

Fig. 5 Photographs of sample sites Reuss-20 to -22. **a** Erratic boulder Reuss-20 on Stetten Stadial moraine near Wohlen, "Erdmannlistein" in the background; **b** "Kleiner Römerstein" (Reuss-22); and **c** "Grosser Römerstein" (Reuss-21). For detail location of Reuss-20 to -22, see Fig. 2

nitric acid. Dissolved samples were then centrifuged and rinsed with ultrapure water to collect all chlorine, and the undissolved part of the sample was separated. Chlorine from the dissolved sample was precipitated as AgCl by addition of $AgNO_3$. Sulphur was precipitated in the form of $BaSO_4$ to avoid high interference of ^{36}Cl with its isobar ^{36}S during the AMS measurement. AMS measurements were done by applying the isotope dilution technique (Synal et al. 1997), measuring both stable Cl isotopes (^{35}Cl and ^{37}Cl) and ^{36}Cl isotope concentrations in one target. The isotope dilution technique gives essential improvements in precision and sensitivity of AMS measurements (Ivy-Ochs et al. 2004b; Desilets et al. 2006), and it allows measurement of total Cl. The $^{36}Cl/Cl$ ratios of the samples were normalized to the ETH internal standard K381/4N with a value of $^{36}Cl/Cl = 17.36 \times 10^{-12}$, and the Table $^{37}Cl/^{35}Cl$ ratios to the natural ratio $^{37}Cl/^{35}Cl = 31.98$ % of K381/4N standard and machine blank. The applied sulphur reduction of measured $^{36}Cl/Cl$ ratios was negligible (0.2–0.5 % of ratios). We corrected the measured sample $^{36}Cl/Cl$ ratios for a procedure blank of 6×10^{-15} that amounted to a correction of less than 2.5 %. For the production rate of cosmogenic ^{36}Cl, we used a Ca spallation of 48.8 ± 1.7 atoms g^{-1} Ca a^{-1} at SLHL in our calculations. For the production of ^{36}Cl due to muon capture a rate of 5.3 ± 0.5 atoms g^{-1} Ca a^{-1} at SLHL (Stone et al. 1996, 1998) was used. The scaling of Stone (2000) is taken into account for site altitude and latitude. Time dependent variations incorporated in our calculations follow Balco et al. (2008). An erosion rate of 5 mm ka^{-1} was assumed for limestone (Rigi-5) and 3 mm ka^{-1} for the more resistant conglomerate boulders. Furthermore, we used a fast neutron attenuation length of 160 g cm^{-2} and rock density of 2.4 g cm^{-3}. For the ^{36}Cl production due to capture of thermal and epithermal neutrons, we follow Liu et al. (1994) and Phillips et al. (2001), using a rate of

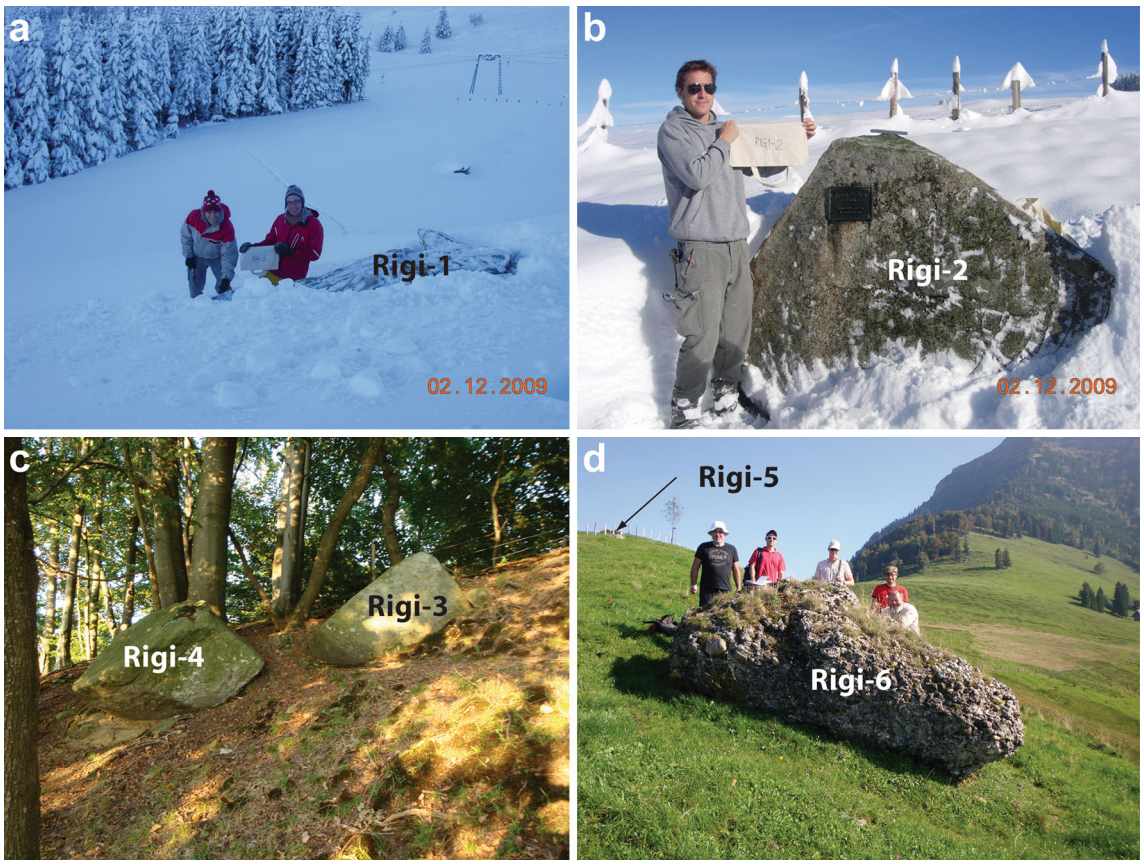

Fig. 6 Photographs of sample sites Rigi-1 to Rigi-6 (for location, see Fig. 4). **a** Boulder Rigi-1; **b** boulder Rigi-2; **c** boulders Rigi-3 and -4; and **d** Boulders Rigi-5 and -6

760 ± 150 neutrons g^{-1} a^{-1} to calculate production of low-energy neutrons above the surface (for details see Alfimov and Ivy-Ochs 2009). For production of ^{36}Cl out of ^{40}K the rate of Evans et al. (1997) is taken for the age calculation. Nevertheless, the effect of this production is negligible in our samples as the concentration of potassium in the dissolved part in all samples is <0.3 % (Online Resource 1).

Major element, gadolinium and samarium concentrations (Online Resource 1) were used to determine the fraction of low-energy neutrons available for capture by ^{35}Cl to form ^{36}Cl (Fabryka-Martin 1988; Phillips et al. 2001; Alfimov and Ivy-Ochs 2009). Uranium and thorium concentrations in our samples are low, <3.7 ppm (Online Resource 1). Thus, the contribution of non-cosmogenic subsurface ^{36}Cl is negligible (Fabryka-Martin 1988). In Table 3, the total weight of the dissolved samples, total Cl concentration, ^{36}Cl concentration per gram rock and erosion corrected exposure ages are listed. The concentration of ^{36}Cl varies from 49.5 ± 2.3 (Rigi-6) to 86.9 ± 3.0 (Rigi-7) 10^6 atoms g^{-1}. The erosion corrected ^{36}Cl exposure ages range from 11.6 ± 0.7 ka (Rigi-6) to 20.4 ± 1.0 ka (Rigi-7).

4 Interpretation of surface exposure ages

4.1 Glacier positions at Lenzburg and Wohlen

The LGM exposure ages from Reuss-22 (22.2 ± 1.0 ka) indicate that the reconstruction of the ice margin at Lenzburg (Fig. 1), based on the mapping of the faint ridges visible on the DEM (Fig. 3), needs revision under consideration of map scales. Within the given uncertainties the ages of Reuss-22 and Reuss-21 (22.0 ± 0.9 ka) are the same. This time match shows that these large boulders (Table 1; Fig. 5) were obviously not affected by the fluvial processes that were active during downmelt and retreat of the glacier. Fluvial modification was probably restricted to breaching of the moraines and the deposition of the next lower level of outwash terraces in the Bünz valley (Fig. 3). Those terrace incisions were probably the latest morphological action during retreat from LGM positions. Boulder Reuss-20 from the retreat stadial in Wohlen yielded an age of 18.6 ± 0.9 ka. This age indicates a retreat from the LGM moraines in Lenzburg to the later frontal position in Wohlen in about 3 ka. We assume that our exposure ages

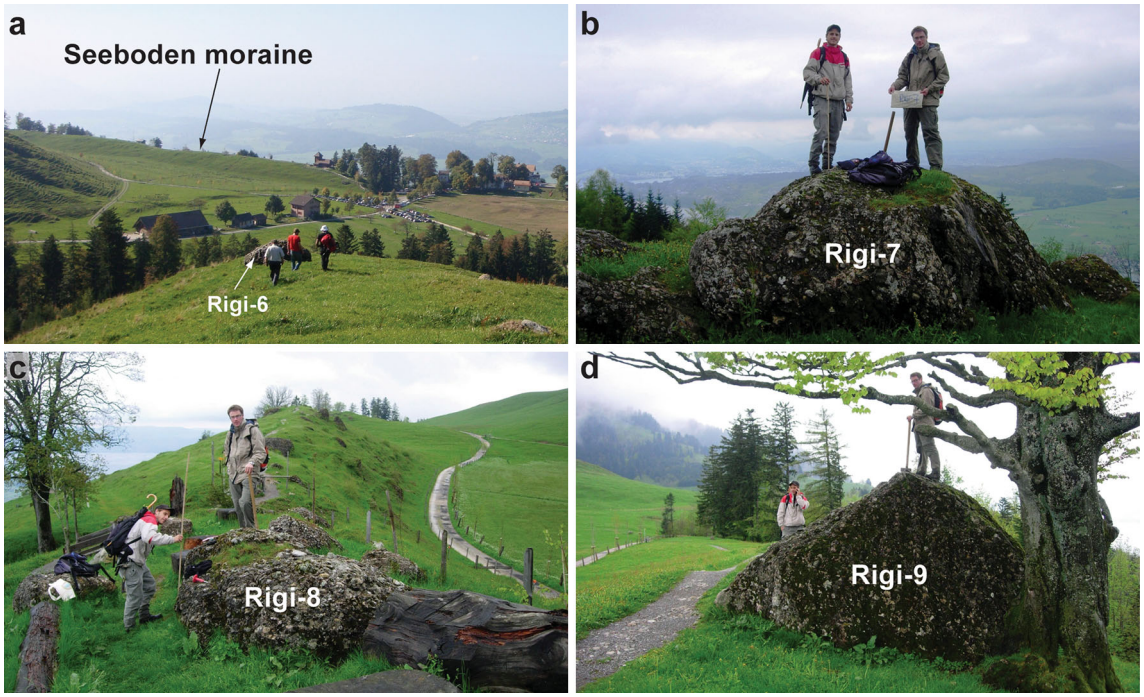

Fig. 7 Photographs of sample sites Rigi-6 to Rigi-9 (for location, see Fig. 4). **a** View from position of boulder Rigi-5 towards Rigi-6, Seeboden moraine visible in background; **b** Boulder Rigi-7; **c** Boulder Rigi-8; and **d** Boulder Rigi-9

are most likely close to their true depositional ages, as post-depositional effects on these boulders seem negligible based on field evidence (such effects have been extensively discussed by Akçar et al. 2011).

4.2 Lateral positions at Rigi

Exposure ages were derived from boulders on the Seeboden moraine ridge, from topographically higher and morphologically complex areas and from recessional moraines topographically lower than the Seeboden moraine.

4.2.1 Boulders from the Seeboden moraine ridge

Boulders Rigi-2, -7, -8 and -9 are situated on the crest of the Seeboden lateral moraine ridge (Figs. 4, 6b, 7b, c). The exposure ages obtained are 7.8 ± 0.4 ka (Rigi-2), 15.6 ± 0.8 ka (Rigi-8), 16.3 ± 0.8 ka (Rigi-9) and 20.4 ± 1.0 ka (Rigi-7). This lateral moraine is characterized by steep slopes; hence, stabilization and degradation can result in the exhumation or slight tilting of the boulders (Porter and Swanson 2008). The boulder localities on this moraine are in contrast with the stable position of the boulders sampled at the frontal position of the Reuss Glacier. At Seeboden, slope instabilities may occur and may likewise result in a cluster of exposure ages (Putkonen and Swanson 2003; Putkonen and O'Neal 2006; Porter and Swanson 2008). However, this clustering of ^{36}Cl ages may also be due to unknown methodological effects of measuring polymict conglomerates on the other hand, vegetation on neighbouring boulders on the same moraine indicates soil formation and erosion which makes the presence of younger ages likely. In addition, weathering of single clasts out of the conglomerate may result in the disintegration of the pebbles, which again may result in younger ages. The significantly younger ^{10}Be age of Rigi-2 (7.8 ± 0.4 ka) probably indicates an anthropogenic effect (see Fig. 6b), as a memorial plate has been placed on the boulder, which is located on the outer side of the Seeboden moraine, and may have moved or tilted.

The Seeboden moraine would have been provided with sediments from the Reuss Glacier until 15.6 ± 0.8 ka in case the exposure ages from Rigi-8 and -9 are considered as true depositional ages. However, this hypothesis of continuous moraine formation until 15.6 ± 0.8 ka is unlikely. Already by 19–18 ka several lines of evidence show that LGM glaciers had retreated behind the Alpine front (Reitner 2007). At 17.1 ± 1.6 ka (recalculated from Ivy-Ochs et al. 2006) late-glacial glaciers were re-advancing to positions well inside the Alpine valleys ("Gschnitz stadial"; Heuberger 1966). For the Reuss Glacier, the Gschnitz correlative moraines (undated up to now) are found in Attinghausen (Spillmann et al. 2011; Att in Fig. 1) which is 60 km up-valley from the retreat position in Wohlen. Our working interpretation is that the younger ages of boulders Rigi-2 (7.8 ± 0.4 ka), Rigi-8

Table 2 Cosmogenic ^{10}Be data and exposure ages of the granitic samples

^{10}Be sample name	Quartz dissolved (g)	^{9}Be spike (mg)	Measured ^{10}Be/^{9}Be × 10^{-14}	AMS error (%)	^{10}Be (10^4 atoms/g)	Exposure age (ka) erosion corrected (ε = 1.0 mm/ka)
Reuss-20	50.3283	0.1943	43.4	4.8	11.16 ± 0.54	18.6 ± 0.9 (1.3)
Reuss-21	50.3933	0.1989	47.3	3.9	12.44 ± 0.49	22.0 ± 0.9 (1.4)
Reuss-22	47.1577	0.1995	46.5	4.4	13.11 ± 0.58	22.2 ± 1.0 (1.5)
Rigi-1	40.2384	0.1994	52.1	4.1	15.64 ± 0.65	16.2 ± 0.7 (1.0)
Rigi-2	40.0631	0.2049	24.4	4.1	7.48 ± 0.33	7.8 ± 0.4 (0.5)
Rigi-3	45.3952	0.1679	32.5	5.7	8.03 ± 0.46	13.0 ± 0.8 (1.0)
Rigi-4	46.3604	0.1678	22.1	5.3	5.36 ± 0.28	8.7 ± 0.5 (0.6)

AMS measurement errors are at 1σ level, including the statistical (counting) error and the error due to normalization of standards and blanks. The error weighted average ^{10}Be/^{9}Be full process blank ratio is (2.90 ± 0.33) × 10^{-15}. Exposure ages are calculated with the CRONUS-Earth exposure age calculator (http://hess.ess.washington.edu/math/; v.2.2; Balco et al. 2009 and were updated from v.1 to v. 2.2 as published by Balco in October 2013). Exposure ages are corrected for shielding of surrounding topography, and sample thickness, as explained in the text; the uncertainties reported in parentheses also include the production rate error. 2.65 g/cm^3 for rock density and a half-live of 1.39 MA for ^{10}Be (Korschineck et al. 2010; Chmeleff et al. 2010) are used for the age calculations

Table 3 Cosmogenic ^{36}Cl data and exposure ages of carbonate and conglomerate samples

^{36}Cl sample name	Weight of sample (g)	Cl conc. in rock (ppm)	^{36}Cl conc. ($\times 10^4$ ^{36} Cl g (Ca)$^{-1}$)	Erosion corrected (ε = 3.0 mm/ka) Exposure age (ka)
Rigi-5	54.5830	12.04 ± 0.07	75.5 ± 3.5	15.4 ± 0.9[a]
Rigi-6	43.6201	46.51 ± 0.85	49.5 ± 2.3	11.6 ± 0.7
Rigi-7	56.2160	42.09 ± 0.35	86.9 ± 3.0	20.4 ± 1.0
Rigi-8	53.5607	33.48 ± 0.23	55.7 ± 2.2	15.5 ± 0.8
Rigi-9	58.4413	13.28 ± 0.05	69.4 ± 2.6	16.3 ± 0.8

Analytical errors are at 1σ level, including the statistical (counting) error and the combined counting uncertainty and the uncertainty due to normalization of standards and blanks. To calculate exposure ages we have used 48.8 ± 1.7 atoms ^{36}Cl g (Ca)$^{-1}$ a^{-1} SLHL production rate from Ca spallation, 5.3 ± 0.5 ^{36}Cl g (Ca)$^{-1}$ a^{-1} SLHL production due to muon capture (Stone et al. 1996, 1998, one sigma errors) and scaled after Stone (2000) to 2.47 (spallation) and 1.61 (muonic) of the SLHL values. Low-energy capture of thermal and epithermal neutrons is computed following Liu et al. (1994) and Phillips et al. (2001) using the production rate of epithermal neutrons above the surface 760 ± 150 neutrons g^{-1} a^{-1} (see Alfimov and Ivy Ochs 2009). Exposure ages are corrected for shielding of surrounding topography and sample thickness

[a] Rigi-5 is a limestone therefore, a higher erosion rate of 5.0 mm/ka is used for calculation

(15.6 ± 0.8 ka) and Rigi-9 (16.3 ± 0.8 ka) on the Seeboden moraine resulted from post-depositional effects.

4.2.2 *Boulders topographically above the Seeboden moraine ridge*

Boulders Rigi-1, -5 and -6 are located topographically higher than the Seeboden moraine (Fig. 4). If they were deposited by the Reuss Glacier lobe, they must have been deposited prior to the deposition of the Seeboden moraine. Rigi-1 (Figs. 4, 6a), Rigi-5 and -6 (Figs. 4, 6d, 7a) are situated at the same altitude (Table 1; Fig. 8), but on two different slopes separated by a small gully (Fig. 4). These two slopes do not belong to a clearly defined glaciomorphological feature. Cautiously, we interpret the calculated exposure ages, which are considerably younger than the LGM (Rigi-1: 16.2 ± 0.7 ka; Rigi-5: 15.5 ± 0.9 ka and Rigi-6: 11.6 ± 0.7 ka) to reflect slope processes and or exhumation during deglaciation.

Bedrock depth here is rather shallow and the slopes are relatively steep and sediment cover of the boulders of more than 2 m for a longer period is difficult to evaluate. The concentrations of the cosmogenic nuclides in the boulder surfaces are too low with a sediment cover of 2 m only to have been deposited prior to 30 ka. For sample Rigi-1, a 50 cm cover of glacial sediment would yield an exposure age of 21 ka. For older glaciations, a considerably higher sediment cover is necessary, e.g. around 1.5 m for 75 ka of exposure based on the measured nuclide concentrations. Although this does not seem impossible, such a scenario is considerably less plausible when applied to Rigi-5 and Rigi-6. To have been originally deposited at 75 ka, Rigi-5 must have been covered by >4 m of sediment and Rigi-6 by >6 m. Therefore, even if deposition of these boulders during an older glaciation (e.g. MIS 4 or 6) seems unlikely, the real original sediment cover cannot be evaluated. The only simple fact we can observe is that boulders Rigi-1 and -5 are lithologies that do not outcrop at Rigi and cannot have been derived locally. Therefore, they must have been transported by the Reuss Glacier and their depositional age must be older than the age of the Seeboden moraine.

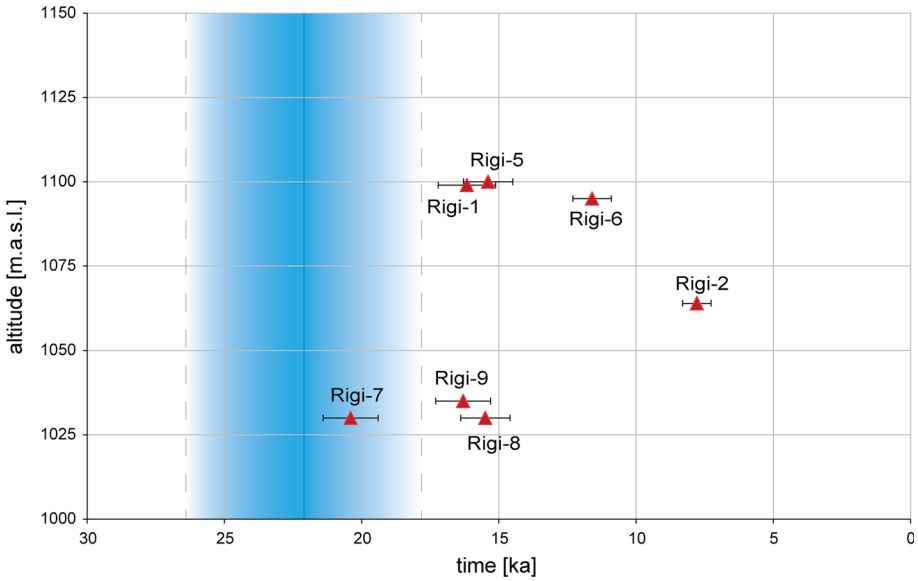

Fig. 8 Plot of the exposure ages for the Reuss Glacier lateral position (Rigi sample sites), with surface exposure ages plotted against altitude. The *shaded area marked* with *dashed lines* is the time window for the northern hemisphere Last Glacial Maximum (LGM) at 22.1 ± 4.3 ka (Shakun and Carlson 2010)

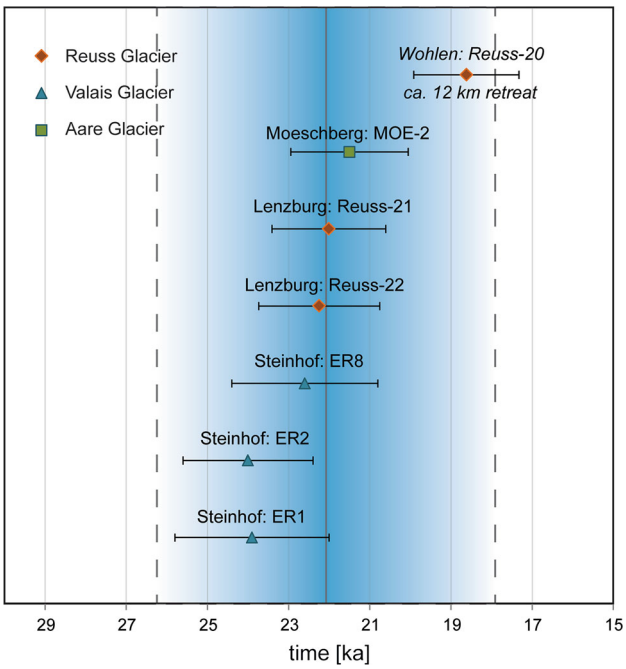

Fig. 9 Compilation of exposure ages from the northern Alpine foreland showing the Reuss Glacier (this study), the Valais Glacier (Ivy-Ochs et al. 2008) and the Aare Glacier (Akçar et al. 2011). Dated boulders are in frontal (terminal) positions. *Shaded area* illustrates the northern hemisphere Last Glacial Maximum (LGM) at 22.1 ± 4.3 ka (Shakun and Carlson 2010)

4.2.3 Boulders topographically lower than the Seeboden moraine ridge

Rigi-3 and -4 are located on a recessional moraine on the steep lower slope (Figs. 4, 6c) below the Seeboden moraine. The exposure ages of 8.7 ± 0.5 ka (Rigi-4) and 13.0 ± 0.8 ka (Rigi-3) suggest that these boulders were most probably, exhumed. The lower slopes of the Rigi are a highly urbanized area (Heim 1919; Hantke 2006; Lüthold 2010), so only a few boulders of clearly erratic origin are available for sampling. However, the minimum age of Rigi-3 (13.0 ± 0.8 ka) seems to be outside the depositional time estimate from the stratigraphic position during deglaciation, even outside the 2 sigma uncertainty limit.

5 Discussion

Evidence for a two-phase LGM advance in the Alps (during MIS 2) has been detected in numerous outcrops across northern Switzerland (Graf 2009 and references therein). The sediments of the Lindmühle advance are correlated with gravel aggradations of the Rafzerfeld (Rafzerfeld Schotter; Rafz in Fig. 1), where these gravels are dated by radiocarbon on mammoth remains to 29 ka (Preusser and Graf 2002). In addition, Graf (2009) suggests that the Lindmühle advance was more extensive in the western part of the northern Alpine foreland compared to the later Birmenstorf advance which may have been more extensive in the eastern part of the foreland. Graf (2009) proposes strong local fluvial erosion (e.g. "Birrfeld-Rinne" and "Fislibach-Birmenstorf-Rinne"), between the two LGM advances. Therefore, the sediments of the later Birmenstorf advance are more likely to be preserved. On the lateral position beyond the LGM Seeboden moraine, Rigi-1, -5 and -6 are boulders dated to address the question of whether or not they originate from a pre-LGM or alternatively from a local LGM glaciation on the Rigi (Fig. 4). Based on our results, both a local LGM advance and an older glaciation are rather unlikely. Firstly, these erratic boulders are from the catchment of the Reuss

Glacier, and are not locally derived. Secondly, they are situated topographically above the LGM Seeboden moraine, which is dated to 20.4 ± 1.0 ka (Rigi-7). Thirdly, although burial by a certain sediment cover is not ruled out, the high amount of sediment required to bring the measured concentrations in accordance with deposition during MIS 4 or 6 is excessive and clear field evidence is lacking. Therefore, we suggest that boulders Rigi-1,-5 and -6 may have been deposited during an early LGM advance, comparable with the Lindmühle advance of Graf (2009). As a consequence, build-up of the pronounced lateral Seeboden moraine would have taken place during the second LGM phase which is the Birmenstorf advance of Graf (2009). In the lateral position on the Rigi geomorphological evidence for the Lindmühle advance, such as moraine ridges, is lacking.

At a broad regional scale we compare the Reuss Glacier with data from the eastern and western Swiss Plateau: A schematic chronology of the LGM of the Rhaetian and Linth Glaciers is given in Keller and Krayss (2005b). They combine lithostratigraphic evidence with calibrated radiocarbon dates, and assume that the main advance of the last glacial cycle occurred just after ca. 30 ka and reached its maximum position at 24–22 ka (Keller and Krayss 2005b, 2010; Preusser et al. 2011). For the Valais Glacier, a radiocarbon date on a mammoth tusk at Finsterhennen (Fig. 1) found in the middle part of glaciofluvial sediments (Schlüchter 2004) is 25,370 ± 190 ^{14}C years (30,600–29,600 cal BP; recalibrated; OxCal 4.2; Bronk Ramsey et al. 2010). This radiocarbon age is in accordance with optical stimulated luminescence (OSL) ages of 28.5 ± 2.3 and 28.9 ± 2.5 ka on surrounding sediments (Preusser et al. 2007).

Our results indicate that the Reuss Glacier started to retreat at 22.2 ± 1.0 ka (Reuss-22) which seems to be synchronous with the retreat of the Valais lobe further to the west, where boulder ER1 at Steinhof (canton Solothurn; Fig. 1) yielded a ^{10}Be exposure age of 24.0 ± 1.1 ka (Ivy-Ochs et al. 2004a, recalculated; Fig. 9). This synchrony is also given for the Aare Glacier with an exposure age on an erratic boulder of 21.5 ± 1.0 ka at Möschberg (Figs. 1, 9; Akçar et al. 2011). Within one sigma uncertainty, the exposure ages for the lobes of the Valais, Aare and Reuss Glaciers (Fig. 1) agree with the age of the global LGM of 22.1 ± 4.3 ka for the northern hemisphere given in Shakun and Carlson (2010).

The Reuss lobe retreated for 12 km to the Stetten Stadial at Wohlen from the frontal position (in 2–3 ka, Reuss-20 = 18.6 ± 0.9 ka; Fig. 2). A rapid ice decay or even collapse of foreland ice (Schlüchter 1988) may have occurred after 18.6 ± 0.9 ka. Late-glacial glacier advances happened only in the high-alpine valleys, e.g. the Gschnitz stadial at 17.1 ± 1.6 ka. The equilibrium line altitude (ELA) is at least 500 m higher during the Gschnitz stadial than during the LGM (Ivy-Ochs et al. 2008 and references therein). For the Reuss Glacier a first indication for the timing of deglaciation at the border of the Alps has been provided: The Seeboden moraine at Rigi indicates that the ice surface reached an elevation of a 1,000 m a.s.l. at 20.4 ± 1.0 ka (Rigi-7). This date pinpoints the onset of deglaciation from a lateral alpine border position. However, the date of 20.4 ± 1.0 ka is within one sigma uncertainty close to 22.2 ± 1.0 ka for the LGM terminal position at Lenzburg. These data point to a simultaneous deglaciation from frontal and lateral position, which requires an active downmelt of the ice.

The northern Alpine foreland was completely free of ice by 18 ka (van Husen 1997; Keller and Krayss 2005b; Ivy-Ochs et al. 2008). For the Valais Glacier (Fig. 1), two sites are important: firstly, at Hauterive/Rouges-Terres (Fig. 1), Hadorn et al. (2002) report an oldest post-LGM radiocarbon date of 14,250 ± 95 ^{14}C years (17,700–16,970 cal BP; recalibrated; OxCal 4.2; Bronk Ramsey et al. 2010) for the northeastern end of Lake Neuchâtel. Secondly, a radiocarbon date of 12,760 ± 100 ^{14}C years (15,870–14,610 cal BP; recalibrated; OxCal 4.2; Bronk Ramsey et al. 2010) indicates an ice-free northern part of Lake Neuchâtel (Magny et al. 2003), situated approximately 60 km upvalley/upglacier from Steinhof—for the Rhaetian and Linth Glacier (Fig. 1), reference is made to the date in Lister (1988) for an ice free Lake Zürich (Lake ZH in Fig. 1) at 14,600 ± 250 ^{14}C years (18,510–17,160 cal BP; recalibrated OxCal 4.2; Bronk Ramsey et al. 2010).

6 Conclusions

We studied lateral and terminal moraines of the LGM piedmont lobe of the Reuss Glacier, and exposure dated numerous erratic boulders with ^{10}Be and ^{36}Cl. We conclude that the exposure ages from the lateral Seeboden moraine on the Rigi indicate an ice surface at an elevation of about 1,000 m a.s.l. up to 20.4 ± 1.0 ka. Our results are not consistent with the hypothesis that the boulders located above and beyond the Seeboden moraine were deposited during MIS 4 or MIS 6. The cosmogenic ^{36}Cl concentrations of the extra-Seeboden moraine boulders are too low to have been acquired after a pre-LGM deposition. It is suggested that these boulders are depositional elements of an earlier phase of the LGM. This phase would then correlate with the Lindmühle advance described in the Alpine foreland by Graf (2009). As a consequence, the formation of the Seeboden moraine took place in the later phase of the LGM (=Birmenstorf advance of Graf 2009). Unfortunately the most likely frontal positions of the Lindmühle and Birmenstorf advances to the Lenzburg area are not yet dated individually (Fig. 3): the dates of Reuss-21 and -22

are the same. The geomorphological observation and dating of a two-phase LGM in the Alps, has been presented by Monegato et al. (2007) for the southern Alpine foreland. The termination of the LGM glaciation was rather abrupt. The date of 18.6 ± 0.9 ka from a recessional moraine near Wohlen of the Reuss Glacier indicates a retreat of about 12 km in 2–3 ka before the final retreat into the high-alpine valleys and the next younger advance (Gschnitz stadial moraines, Ivy-Ochs et al. 2006).

A first methodological experiment to exposure-date boulders on post-LGM moraines on the northern slope of the Rigi below the Seeboden moraine has brought what is most likely evidence of post-depositional processes. The latter are attributed to intense land use over millennia as well as to primary affects associated with moraine stabilization and degradation. A second methodological experiment to measure concentrations of ^{36}Cl in polymictic Molasse conglomerates has been successful (Rigi-6 to -9). This advance in surface exposure application opens new possibilities in the selection of lithologies for this dating technique.

Acknowledgments We would like to thank the Accelerator Mass Spectrometry (AMS) facility operated by the Swiss Federal Institute of Technology (ETH), Zürich, Switzerland. This study was funded by the Swiss National Science Foundation (Project No. 200020-125203). Special thanks go to the reviewers of this paper for their constructive comments.

References

Akçar, N. (2006). Paleoglacial records from the black sea area of Turkey field and dating evidence. *Ph.D. Thesis*, Bern University, Bern, Switzerland.

Akçar, N., Deline, P., Ivy-Ochs, S., Alfimov, V., Hajdas, I., Kubik, P. W., et al. (2012). The 1717 AD rock avalanche deposits in the upper Ferret Valley (Italy): A dating approach with cosmogenic 10Be. *Journal of Quaternary Science, 27*, 383–392.

Akçar, N., Ivy-Ochs, S., Kubik, P. W., & Schlüchter, C. (2011). Post-depositional impacts on 'Findlinge' (erratic boulders) and their implications for surface exposure dating. *Swiss Journal of Geosciences, 104*, 445–453.

Alfimov, V., & Ivy-Ochs, S. (2009). How well do we understand production of ^{36}Cl in limestone and dolomite? *Quaternary Geochronology, 4*(6), 462–474.

André, M.-F. (2002). Rates of postglacial rock weathering on glacially scoured outcrops (Abisko-Riksgransen area, 68 degrees N). *Geografiska Annaler, 84A*, 139–150.

Balco, G., Briner, J., Finkel, R. C., Rayburn, J. A., Ridge, J. C., & Schaefer, J. M. (2009). Regional beryllium-10 production rate calibration for northeastern North America. *Quaternary Geochronology, 4*, 93–107.

Balco, G., Stone, J. O., Lifton, N. A., & Dunai, T. J. (2008). A complete and easily accessible means of calculating surface exposure ages or erosion rates from Be-10 and Al-26 measurements. *Quaternary Geochronology, 3*, 174–195.

Baltzer, A. (1896). Der diluviale Aargletscher und seine Ablagerungen in der Gegend von Bern mit Berücksichtigung des Rhonegletschers. Schmid, Bern. Beiträge zur geologischen Karte der Schweiz 30.

Beck, P. (1933). *Chronologie der schweizerischen Eiszeiten*. Thun: Lith. Casserini & Aebi.

Bini, A., Buoncristiani, J.-F., Couterrand, S., Ellwanger, D., Felber, M., Florineth, D., et al. (2009). *Die Schweiz während des letzteiszeitlichen Maximums (LGM) 1:500 000*. Bern: Federal Office of Topography, swisstopo.

Briner, J. P., Young, N. E., Goehring, B. M., & Schaefer, J. M. (2012). Constraining Holocene 10Be production rates in Greenland. *Journal of Quaternary Science, 27*, 2–6.

Bronk Ramsey, C., Dee, M., Lee, S., Nakagawa, T., & Staff, R. A. (2010). Developments in the Calibration and Modeling of Radiocarbon Dates. *Radiocarbon, 52*(3), 953–961.

Chmeleff, J., von Blanckenburg, F., Kossert, K., Gerstmann, U.C., Knie, K., Rugel., G., Wallner, A., Dillmann, I., Dollinger, G., Lierse von Gostomski, Ch., Kossert, K., Maiti, M., Poutivtsev, M., Remmert, A. (2010). Determination of the Be-10 half-life by multicollector ICP-MS and liquid scintillation counting. *Nuclear Instruments and Methods in Physics Research Section B*, *268*, 192–199.

Clark, P. U., Dyke, A. S., Shakun, J. D., Carlson, A. E., Clark, J., Wohlfarth, B., et al. (2009). The last glacial maximum. *Science, 325*, 710–713.

Desilets, D., Zreda, M., Almasi, P. F., & Elmore, D. (2006). Determination of cosmogenic Cl-36 in rocks by isotope dilution: innovations, validation and error propagation. *Chemical Geology, 233*(3–4), 185–195.

Dunai, T. J. (2010). *Cosmogenic nuclides principles, concepts and applications in the earth surface sciences*. Cambridge: Cambridge University Press.

Dunne, J., Elmore, D., & Muzikar, P. (1999). Scaling factors for the rates of production of cosmogenic nuclides for geometric shielding and attenuation at depth on sloped surfaces. *Geomorphology, 27*, 3–11.

Ellwanger, D., Fiebig, M, Heinz, J. mit Beiträgen zur Pollenanalyse von BLUDAU, W. (1999). Quartärgeologie des mittleren Rheingletschergebietes (Bittelschiess, Höchsten, Hosskirch, Ostrach). *Jahrbuch und Mitteilungen des Oberrheinischen Geologischen Vereins, Neue Folge*, *81*, 217–230.

Evans, J. M., Stone, J. O. H., Fifield, L. K., & Cresswell, R. G. (1997). Cosmogenic chlorine-36 production in K-feldspar. *Nuclear Instruments and Methods in Physics Research Section B-Beam Interactions with Materials and Atoms, 123*, 334–340.

Fabryka-Martin, J.T. (1988). Production of radionuclides in the earth and their hydrogeologic significance, with emphasis on Chlorine-36 and Iodine-129. *Ph.D. Thesis*, University of Arizona, Tucson, USA.

Fenton, C. R., Hermanns, R. L., Blikra, L. H., Kubik, P. W., Bryant, C., Niedermann, S., et al. (2011). Regional ^{10}Be production rate calibration for the past 12 ka deduced from the radiocarbon-dated Grøtlandsura and Russenes rock avalanches at 69° N, Norway. *Quaternary Geochronology, 6*, 437–452.

Florineth, D., & Schlüchter, C. (1998). Reconstructing the Last Glacial Maximum (LGM) ice surface geometry and flowlines in the Central Swiss Alps. *Eclogae Geologicae Helvetiae, 91*, 391–407.

Goehring, B. M., Lohne, Ø. S., Mangerud, J., Svendsen, J. I., Gyllencreutz, R., Schaefer, J., et al. (2012). Late glacial and holocene 10Be production rates for western Norway. *Journal of Quaternary Science, 27*, 89–96.

Graf, H.R. (2009). Stratigraphie von Mittel- und Spätpleistozän in der Nordschweiz. Beiträge zur Geologischen Karte der Schweiz, 168, Federal Office of Topography swisstopo, Wabern.

Hadorn, P., Thew, N., Coope, G.R., Lemdahl, G., Hajdas, I., Bonani, G. (2002). A Late-Glacial and early Holocene environment and

climate history for the Neuchâtel region (CH). In H. Richard, A. Vignot (Eds.), Equilibres et Ruptures dans les Ecosystèmes depuis 20 000 ans en Europe de l'Ouest. Collection Annales Littéraires; Série. Environment, Sociétés et Archéologie (Vol. 3, pp. 75–90).

Hantke, R. (1983). Eiszeitalter Band 3. Ott Verlag, Thun; 1992 Eiszeitalter 1-3, ecomed, Landsberg/Lech.

Hantke, R. (2006). Blatt 1151 Rigi, mit Nordteil von Blatt 1171 Beckenried. Geologischer Atlas Schweiz 1:25000, Erläuterungen 116. Bundesamt für Landestopografie: Wabern-Bern.

Hantke, R. (2011). *Eiszeitalter: Kalt-/Warmzeit-Zyklen und Eistransport im alpinen und voralpinen Raum*. Bern: Ott.

Heim, A. (1919). Geologie der Schweiz. Tauchnitz, Leipzig, Band 2, Hälfte 1. Die Schweizer Alpen.

Heuberger, H. (1966). Gletschergeschichtliche Untersuchungen in den Zentralalpen zwischen Sellrain-und Ötztal. Wissenschaftliche Alpenvereinshefte (Vol. 20). Universitätsverlag Wagner, Innsbruck.

Hippe, K., Ivy-Ochs, S., Kober, F., Zasadni, J., Wieler, R., Wacker, L., et al. (2014). Chronology of Lateglacial ice flow reorganization and deglaciation in the Gotthard Pass area, Central Swiss Alps, based on cosmogenic ^{10}Be and in situ^{14}C. *Quaternary Geochronology, 19*, 14–26.

Ivy-Ochs, S., Kerschner, H., Kubik, P. W., & Schlüchter, C. (2006). Glacier response in the European Alps to Heinrich event 1 cooling: The Gschnitz stadial. *Journal of Quaternary Science, 21*, 115–130.

Ivy-Ochs, S., Kerschner, H., Reuther, A., Preusser, F., Heine, K., Maisch, M., et al. (2008). Chronology of the last glacial cycle in the European Alps. *Journal of Quaternary Science, 23*(6–7), 559–573.

Ivy-Ochs, S., Kober, F. (2008). Surface exposure dating with cosmogenic nuclides. *E&G—Quaternary Science Journal*, *57*, 1–2, 179–209.

Ivy-Ochs, S., Schlüchter, C., Kubik, P. W., Synal, H.-A., Beer, J., & Kerschner, H. (1996). The exposure age of an Egesen moraine at Julier Pass, Switzerland, measured with the cosmogenic radionuclides ^{10}Be, ^{26}Al and ^{36}Cl. *Eclogae Geologicae Helvetiae, 89*(3), 1049–1063.

Ivy-Ochs, S., Schafer, J., Kubik, P. W., Synal, H. A., & Schlüchter, C. (2004a). Timing of deglaciation on the northern Alpine Foreland (Switzerland). *Eclogae Geologicae Helvetiae, 97*, 47–55.

Ivy-Ochs, S., Synal, H.-A., Roth, C., & Schaller, M. (2004b). Initial results from isotope dilution for Cl and Cl-36 measurements at the PSI/ETH Zurich AMS facility. *Nuclear Instruments and Methods in Physics Research B, 223–24*, 623–627.

Jäckli, H. (1962). Die Vergletscherung der Schweiz im Würmmaximum. *Eclogae Geologicae Helvetiae, 55*(2), 285–294.

Jäckli, H. (1966). Blatt 1090 Wohlen. Geologischer Atlas der Schweiz 1:25 000, Erläuterung 50. Bundesamt für Landestopographie: Wabern-Bern.

Jäckli, H. (1970). *Die Schweiz zur letzten Eiszeit, Karte 1:550 000, Atlas der Schweiz, Blatt 6*. Bundesamt für Landestopographie: Wabern-Bern.

Keller, O., & Krayss, E. (2005a). Der Rhein-Linth Gletscher im letzten Hochglazial. 1. Teil: Einleitung: Aufbau und Abschmelzen des Rhein-Linth-Gletschers im Oberen Würm. *Vierteljahresschrift der Naturforschenden Gesellschaft in Zürich, 150*, 19–32.

Keller, O., & Krayss, E. (2005b). Der Rhein-Linth Gletscher im letzten Hochglazial. 2. Teil: Datierung und Modelle der Rhein-Linth-Vergletscherung, Klimarekonstruktionen. *Vierteljahresschrift der Naturforschenden Gesellschaft in Zürich, 150*, 69–85.

Keller, O., & Krayss, E. (2010). Mittel-und spätpleistozäne Stratigraphie und Morphogenese in Schlüsselregionen der Nordschweiz. *Quaternary Science Journal, 59*(1–2), 88–119.

Kelly, M. A., Buoncristiani, J.-F., & Schlüchter, C. (2004). A reconstruction of the last glacial maximum (LGM) ice-surface geometry in the western Swiss Alps and contiguous Alpine regions in Italy and France. *Eclogae Geologicae Helvetiae, 97*, 57–75.

Kohl, C. P., & Nishiizumi, K. (1992). Chemical isolation of quartz for measurement of in situ produced cosmogenic nuclides. *Geochimica Cosmochimica Acta, 56*, 3583–3587.

Kopp, J. (1953). Die Lokalvergletscherungen der Rigi. *Eclogae Geologicae Helvetiae, 46*(2), 237–238.

Korschinek, G., Bergmaier, A., Faestermann, T., Gerstmann, U. C., Knie, K., Rugel, G., Wallner, A., Dillmann, I., Dollinger, G., Lierse von Gostomski, Ch., Kossert, K., Maiti, M., Poutivtsev, M., Remmert, A. (2010). A new value for the half-life of Be-10 by heavy-ion elastic recoil detection and liquid scintillation counting. *Nuclear Instruments and Methods in Physics Research Section B: Beam Interactions with Materials and Atoms*, *268*, 187–191.

Krüger, T. (2008). *Die Entdeckung der Eiszeiten: Internationale Rezeption und Konsequenzen für das Verständnis der Klimageschichte*. Basel: Schwabe.

Lal, D. (1988). Insitu – Produced cosmogenic isotopes in terrestrial rocks. *Annual Review of Earth and Planetary Sciences, 16*, 355–388.

Lal, D. (1991). Cosmic ray labeling of erosion surfaces: In situ nuclide production rates and erosion models. *Earth and Planetary Science Letters, 104*, 424–439.

Lambeck, K., & Chappell, J. (2001). Sea level change through the last glacial cycle. *Science, 292*, 679–686.

Lister, G. S. (1988). A 15,000-year isotopic record from Lake Zürich of deglaciation and climatic change in Switzerland. *Quaternary Research, 29*, 129–141.

Liu, B. L., Phillips, F. M., Fabryka-Martin, J. T., Fowler, M. M., & Stone, W. D. (1994). Cosmogenic ^{36}Cl accumulation in unstable landforms, 1. Effects of the thermal neutron distribution. *Water Resources Research, 30*(11), 3115–3125.

Lüthold, A. (2010). Die Rigi und die letzte Eiszeit, inklusive quartärgeologische Karte 1: 10'000. *M.Sc. Thesis*, University of Bern, Switzerland.

Magny, M., Thew, N., & Hadorn, P. (2003). Late-glacial and early Holocene changes in vegetation and lake-level at Hauterive/Rouges-Terres, Lake Neuchâtel (Switzerland). *Journal of Quaternary Science, 18*, 31–40.

Mix, A. C., Bard, E., & Schneider, R. (2001). Environmental processes of the ice age: land, oceans, glaciers (EPILOG). *Quaternary Science Reviews, 20*, 627–657.

Monegato, G., Ravazzi, C., Donegana, M., Pini, R., Calderoni, G., & Wick, L. (2007). Evidence of a two fold-glacial advance during the last glacial maximum in the Tagliamento end moraine system (eastern Alps). *Quaternary Research, 68*, 284–302.

Penck, A., Brückner, E. (1901/1909). Die Alpen im Eiszeitalter. Tauchnitz: Leipzig.

Phillips, F. M., Stone, W. D., & Fabryka-Martin, J. T. (2001). An improved approach to calculating low-energy cosmic-ray neutron fluxes near the land/atmosphere interface. *Chemical Geology, 175*, 689–701.

Phillips, F. M., Zreda, M. G., Smith, S. S., Elmore, D., Kubik, P. W., & Sharma, P. (1990). Cosmogenic chlorine-36 chronology for glacial deposits at Bloody Canyon. *Eastern Sierra Nevada: Science, 248*, 1529–1532.

Porter, S. C., & Swanson, T. W. (2008). ^{36}Cl dating of the classic Pleistocene glacial record in the northeastern Cascade Range. *Washington, American Journal of Science, 308*, 130–166.

Preusser, F., Blei, A., Graf, H. R., & Schlüchter, C. (2007). Luminescence dating of Würmian (Weichselian) proglacial

sediments from Switzerland: methodological aspects and stratigraphical conclusions. *Boreas, 36*, 130–142.

Preusser, F., Graf, H.R. (2002). Erste Ergebnisse von Lumineszenzdatierungen eiszeitlicher Ablagerungen der Nordschweiz. Jahrbuch und Mitteilungen des Oberrheinischen Geologischen Vereins (Vol. 107, pp. 419–438).

Preusser, F., Graf, H. R., Keller, O., Krayss, E., & Schlüchter, C. (2011). Quaternary glaciation history of northern Switzerland. *Eiszeitalter & Gegenwart Quaternary Science Journal, 60*, 282–305.

Putkonen, J., & O'Neal, M. (2006). Degradation of unconsolidated Quaternary landforms in the western North America. *Geomorphology, 75*, 408–419.

Putkonen, J., & Swanson, T. (2003). Accuracy of cosmogenic ages for moraines. *Quaternary Research, 59*, 255–261.

Reitner, J. M. (2007). Glacial dynamics at the beginning of Termination I in the Eastern Alps and their stratigraphic implications. *Quaternary International, 164*, 64–84.

Schlüchter, C. (1988). The deglaciation of the Swiss Alps: A paleoclimatic event with chronological problems. *Bulletin de l'Association Française pour l'Étude du Quaternaire*, *1988*, 2/3, 141–145.

Schlüchter, C. (2004). The Swiss glacial record—A schematic summary. In J. Ehlers, P.L. Gibbard (Eds.), Quaternary Glaciations—Extent and Chronology. Part I: Europe (pp. 413–418). Amsterdam: Elsevier.

Schlunegger, F., Matter, A., Burbank, D., & Klaper, E. (1997). Magnetostratigraphic constraints on relationships between evolution of the central Swiss Molasse basin and Alpine orogenic events. *Geological Society of America Bulletin, 109*, 225–241.

Shakun, J. D., & Carlson, A. E. (2010). A global perspective on Last Glacial Maximum to Holocene climate change. *Quaternary Science Reviews, 29*, 1801–1816.

Spillmann, P., Naturforschende Gesellschaft Uri (2011). Geologie des Kantons Uri. Naturforschende Gesellschaft Uri, Altdorf 24, 224 pp.

Starnberger, R., Rodnight, H., & Spötl, C. (2011). Chronology of the Last Glacial Maximum in the Salzach palaeoglacier area (Eastern Alps). *Journal of Quaternary Science, 26*, 502–510.

Stone, J. O. (2000). Air pressure and cosmogenic isotope production. Journal of Geophysical Research – Solid. *Earth, 105*, 23753–23759.

Stone, J. O., Allan, G. L., Fifield, L. K., & Cresswell, R. G. (1996). Cosmogenic chlorine-36 from calcium spallation. *Geochimica et Cosmochimica Acta, 60*, 679–692.

Stone, J. O. H., Evans, J. M., Fifield, L. K., Allan, G. L., & Cresswell, R. G. (1998). Cosmogenic chlorine-36 production in calcite by muons. *Geochimica et Cosmochimica Acta, 62*, 433–454.

Synal, H.-A., Bonani, G., Dobeli, M., Ender, R. M., Gartenmann, P., Kubik, P. W., et al. (1997). Status report of the PSI/ETH AMS facility. *Nuclear Instruments and Methods in Physics Research B: Beam Interactions with Materials and Atom, 123*, 62–68.

Van Husen, D. (1997). LGM and Late-glacial fluctuations in the Eastern Alps. *Quaternary International, 38*(39), 109–118.

Young, N. E., Schaefer, J. M., Briner, J. P., & Goehring, B. M. (2013). A 10Be production-rate calibration for the Arctic. *Journal of Quaternary Science, 28*(5), 515–526.